DOI: 10.21062/mft.2022.060 http://www.journalmt.com

Research on the Measurement of Thermal Deformation of Tools on High-speed Machining Centers Based on Image Processing Technology

Changlong Zhao (0000-0001-7778-3494), Ming Li (0000-0003-4202-0256), Junbao Yang (0000-0002-4958-6546), Chen Ma (0000-0002-4884-235X), Zhenrong Ma (0000-0001-6300-2300)
College of mechanical and vehicle engineering, Changchun University, Changchun 130022. Changlong Zhao, China. E-mail: zhao19790204@126.com; 366633219@qq.com

In order to improve the efficiency of high-speed machining center and shorten its warm-up time, it is realistic and feasible to measure the thermal deformation of the machine tool system and then improve the machining accuracy of the machine by means of compensation. In this paper, a model XKA714B/A CNC milling machine and a 10mm diameter ball-head milling tool are selected. A high-speed camera is used to capture the gray level images of the tool when the machining center spindle speed is working at 1000 r/min. Using MATLAB software, the image edge extraction is coarsely localized by Canny algorithm, and sub-pixel fitting edge detection method is used to precisely locate the tool edge profile. The least-squares method is applied to fit the tool tip circular curve so as to calculate the thermal deformation during the tool preheating process. The results showed that there is a certain connection between the thermal deformation of the tool and the machine running time during the preheating process of the machine tool. That is, in the initial stage of machine operation, the tool axial thermal deformation is larger. In the 6th to 26th min, the tool thermal deformation gradually becomes smaller. At the 26th minute of preheating, the tool deformation reached more than 96% of the total deformation and the deformation rate leveled off. The axial deformation of the tool was measured to be 130.2 um at this time. Inputting the measurement results into the machining center tool holder control system as the compensation value will shorten the machine warm-up and thermal balance time so as to ensure its machining accuracy, which is of practical significance to improve machining efficiency and reduce cost in the actual production process.

Keywords: Thermal deformation of tools, Image processing, Edge Extraction, Least squares method

1 Introduction

Following the increasing popularity of information and intelligence in machining, the CNC machine tool has become an important core equipment for precision and ultra-precision machining technology. The industrial sector has also put forward higher requirements for its machining accuracy, while the CNC machine tool error is the primary obstacle that restricts machining accuracy[1-4]. Due to the mechanical structure, processing environment, tool wear, noise and temperature changes, etc., multiple factors coupled together, the CNC machine tools in the process of cutting metal parts will reduce the machine tool machining accuracy, which will also have a certain impact on the quality of parts processing[5-7].Related studies have shown that up to 75% of errors on manufactured work pieces are caused by thermal errors in the machine tool. This deformation can further make the relative position relationship between the tool and the work piece change, which has a significant impact on the accuracy of the machine tool. Whereas the thermal errors caused by the spindle account for approximately 50-80% of the total thermal errors[8-11]. One of the main reasons for this is that when a high-speed machining centre is preheated at a high spindle speed, the tool and the spindle system generate frictional heat due to the high speed of rotation, which causes the tool to deform thermally accordingly.Therefore, the study of thermal deformation measurement of CNC machine tools and the control of thermal deformation compensation is of great significance to improve the accuracy of machine tools.

Over the years, a large number of research results have been obtained by domestic and foreign scholars in the study of thermal deformation. Marcelo O. dos Santos, Gilmar F. Batalha, Ed C. Bordinassi &Gelson F. Miori [12]modelled and analyzed the thermal error of a five-axis CNC machining centre from the estimated temperature field, culminating in an artificial neural network (ANN) algorithm model to accurately and robustly predict the thermal error.Ye, W. H., Guo, Y. X., Zhou, H. F., Liang, R. J. & Chen, W. F.[13]reveal that the value of the thermal deformation coefficient is an important factor affecting the accuracy of a dynamic axis feeding system. The authors measure thermal errors by means of a sensor approach and

propose a new modelling method that can be easily extended to other machine tools. Lambiase, F., Paoletti, A., & Di Ilio, A.[14]measured the temperature by means of an infrared camera and observed a significant increase in temperature during the preheating process, which resulted in a change in the forces acting on the milling machine. Yue, H. T., Guo, C. G., Li, Q., Zhao, L. J., & Hao, G. B.[15]established a model for predicting the thermal errors of machine tool spindle systems under load machining conditions, and verified through experiments that the model has high prediction accuracy and engineering application value.

This paper uses image measurement techniques to measure thermal deformation during the preheating phase of a tool. Illuminated by a special light source for high-speed cameras, capturing the image of the tool by a high-speed camera. Using MATLAB software, the tool images acquired by the high-speed camera are pre-processed with median filtering, histogram equalization and binarization. Using Canny operators in combination with sub-pixel fitting algorithms to obtain accurate contour profiles of tool edges. So we can calculate the tool thermal deformation more accurately, then inserting thermal deformation values into the tool holder motion control for thermal error compensation. Through experimental verification, the amount of tool thermal deformation and machine running time has a certain relationship, when the tool reaches thermal stability, the amount of tool thermal deformation gradually tends to be stable. This method of measuring tool thermal deformation allows for shorter warm-up times before or during tool changes, effectively improving machining accuracy on precision high-speed CNC machines. The study can effectively shorten the tool warm-up time in actual production machining. It improves the accuracy of tool heat deformation measurement, reduces the machining errors caused by thermal errors in actual production machining, and further improves the efficiency and machining accuracy of machining centers.

2 Overall structure of the tool thermal deformation measurement system

During the preheating of the milling tool, image processing is used to transfer the tool image to the PC through a hardware platform built with light sources and high-speed cameras[16]. By processing the acquired image with an operator, the final pre-processed image of the tool is obtained, that allows for edge detection of the tool[17]. The general framework of the measurement experiment platform is shown in Fig. 1.

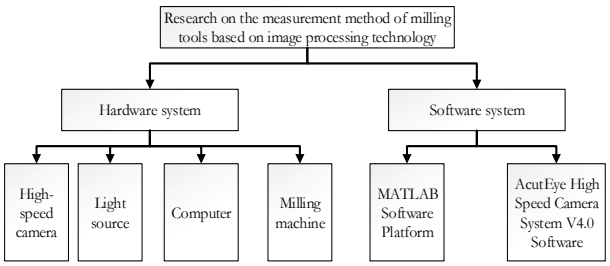

Fig. 1 *General framework of the measurement experiment platform*

2.1 Construction of the measurement system

The measurement method of milling cutter based on image processing technology. The experimental object of the study is a 10mm diameter ball-ended milling cutter, and the experimental platform is mainly composed of two parts: hardware and software (as shown in Fig. 2-Fig. 5).

Fig. 2 *Light source and high-speed camera*

Fig. 3 *XKA714B/A CNC Milling Machine*

Fig. 4 *Milling machine working process*

Fig. 5 *High-speed camera working process*

The hardware part includes a high-speed camera, camera bracket, light source and computer as well as the experimental model XKA714B/A CNC milling machine. The camera is a high-speed camera produced by a company, which can directly collect the gray-scale image of the tool when working. The light source is the point light source equipped by the camera factory, the main function is to provide the necessary lighting, which is installed next to the camera lens. The software part of the system contains the AcutEye High Speed Imaging System V4.0 software, which serves to control the camera and thus enable the imaging acquisition process. The second part is the Matlab software, which is used to fit the acquired data, thus enabling the process of processing the images.

2.2 Camera calibration

Camera calibration is a conversion from the world coordinate system to the camera coordinate system, and then to the image coordinate system[18]. The process of camera calibration is a key part of assuring the accuracy of the measurement results. High-speed cameras use pixels as a unit of measurement in the imaging process, usually reflecting the information and position of an object in two dimensions[19].The steps of the reference calibration method are as follows:

- (1) Select the ball-ended milling cutter to be measured as the calibration reference, and record the outer radius of the milling cutter as $r(\mu m)$.
- (2) Measured at normal room temperature. Firstly, determining the chosen reference, then photographing it with a high-speed camera, and technically processing the acquired image information to obtain the radius dimensions in pixel units, recorded as r_p .
- (3) Calculate the calibration coefficients for the camera using the formula (Equation 1). The equation gives the calibration factor of the camera as the ratio of pixels to true size.
- (4) Storage of the acquired values. This is applied when subsequently the tool is measured.

The sample part chosen for this experimental study is a ball-ended milling cutter with a diameter of 10 mm and a radius of $5000\mu m$. After fixing the high-speed camera and the ball-ended milling cutter, calculating the images gives the diameter r_p in pixel, which gives a calibration factor of k:

$$k = r/r_p \tag{1}$$

In order to achieve a certain improvement in the accuracy of the camera calibration. In this study, a total of six measurements were made on the calibration results, which are then presented separately (as shown in Tab. 1). Reducing the measurement error by averaging it as the final camera calibration value.

Tab. 1 *Measurements of calibration reference detection values (in pixels)*

Groups	1	2	3	4	5	6	Average
Dimensions (*pixel*)	47.26788	44.97985	46.79836	44.99859	45.95876	45.98732	45.99846

Based on the test data in Table 1, it shows that r_p= 45.99846, The calibration factor k for this system is calculated from publication 1 as 108.69929.

3 Sampling and quantifying of tool images

For the measurement of the size of the thermal deformation of the tool, the raw image of the tool is acquired using a high-speed camera with the assistance of a special light source illumination system for high-speed cameras, which in turn quantifies the sampled image. The gray value of the sampled pixels to be acquired is transformed from an analogue to a discrete quantity, which prepares for the subsequent edge extraction of the tool image[20].

3.1 Sampling of tool images

The image sampling process is achieved by means of a sensor elements that convert the individual pixel luminosity captured in the image into a corresponding voltage value, showing a positive correlation between the voltage value and the pixel luminosity[21].

Dot matrix sampling is achieved by taking a sample of a two-dimensional function of the image, by analyzing and reading the signal values of all the discrete points of the image, arranging the results and finally forming an array.

The orthogonal coefficient is an algorithm which transforms the image function acquired during the sampling process. The correlation coefficients obtained by the transformation are used as input values for the sampling of the image.

In the array of $f(x,y)$, assume that the number of images is M x N, the number of horizontal pixels of the array is M and the number of vertical pixels of the array is N. The image pixel expression is shown in Equation 2.

$$f(x,y)=\begin{bmatrix} f(0,0) & f(0,1) & \cdots & f(0,N-1) \\ f(1,0) & f(1,1) & \cdots & f(1,N-1) \\ \cdots & \cdots & \cdots & \cdots \\ f(M-1,0) & \cdots & \cdots & f(M-1,N-1) \end{bmatrix} \quad (2)$$

In the process of image sampling, the sampling input value can be determined in two ways. The first way is to cover the image to be processed with a grid, the brightness of the image is simulated by means of an overlay grid, which takes its mid-point value as the image brightness sampling value, that is, the average value of each grid. The second way is to simulate the lightness value of the image, this is expressed by the intersection of each cell, the value of that intersection being the lightness value of the image.

The sampling process for moving images is the process of sampling an image over a continuous period of time. That is, it is sampled on the time axis, first along the vertical and then along the horizontal, completing the final sampling in the above order. For the rule of sampling interval selection for dynamic images, Assume that ω is the maximum angular frequency of a one-dimensional signal g(t) with a sampling interval of $T \leq 1/2\omega$.

3.2 Quantification of tool images

The process of quantizing a sampled image is the process of taking the acquired gray value of a sampled pixel and realizing its transformation from an analogue quantity to a discrete quantity. The letter z is used to denote the continuous gray scale value of the sampled image, and its range of values should satisfy $z_i \leq z \leq z_{i+1}$, q_i is the quantified value for obtaining the gray scale value of the sampled image pixels. The quantification error is$|z-q_i|$.

Typically, the quantization of images is achieved by means of equal interval quantization. This is the process of quantizing the sampled values by dividing them into equal intervals. The following principles should be followed when quantizing sampled values at equal intervals.

(1) In the case of moving images with changing edges, the number of samples should be reduced to a certain extent and the quantization level should be increased to avoid false outlines in the image.

(2) In the case of more details in a moving image, it should be treated in the opposite way to the case of changing edges, by increasing the number of samples to a certain extent and reducing the quantization level so as to avoid image overlap.

Set the machine spindle speed to 1000r/min and run for the 16th minute, using a high-speed camera to capture images as shown in Fig. 6.

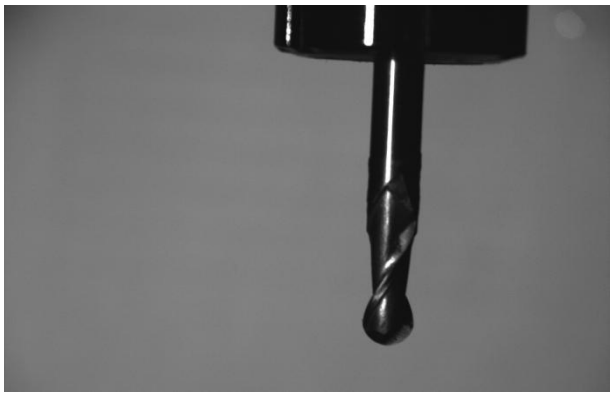

Fig. 6 *Original image of the tool*

4 Tool image processing and thermal deformation measurement

For the measurement of the size of the thermal deformation of the tool, firstly the original image of the tool is captured using a high-speed camera with the assistance of a special light source illumination system. Secondly, the images transferred to the computer are processed using MATLAB software. Finally the extracted edge profiles of the tool are obtained and the

exact value of the tool thermal deformation is calculated. The algorithm flow for the thermal deformation amount is shown in Fig. 7.

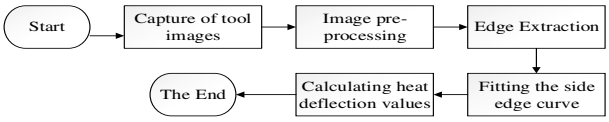

Fig. 7 *Algorithmic process for thermal deformation*

4.1 Tool images processing

In the process of acquiring and transmitting information from digital images, a certain amount of noise is usually generated, of which pretzel noise and Gaussian noise are two of the more common types of noise in the digital images processing[22]. Of these two types of noise, pretzel noise represents a mixture of black noise and white noise, while Gaussian noise is due to noise pollution produced by the internal components of the camera, such as sensors, during its operation[23]. To reduce noise pollution, they have to be de-noised. There is no need to greyscale the images as they are taken by high-speed cameras.

In specific image de-noising, mathematical morphology is used as the theoretical basis. This enables the dimensions and shapes of the structural elements to be determined more quickly. Thus enhancing the filtering effect to a certain extent. In the process of de-noising images with more complex structural elements, the selection of the structural elements requires further consideration. By analyzing the noise characteristics, the element dimensions can be sorted and then processed one by one, from smallest to largest. Thus achieving the effect of reducing noise interference. Therefore, it is scientific and reasonable to use a series of filters to process complex multi-dimensional structural elements in the process of image filtering, which also allows the maximum preservation of the geometric features of the acquired images.

The medfilt2 function is called in Matlab to perform median filtering on the images (the calling procedure is shown in Fig. 8). Then call the filter2 function to process the image with the average filtering (call the procedure in Fig. 9).

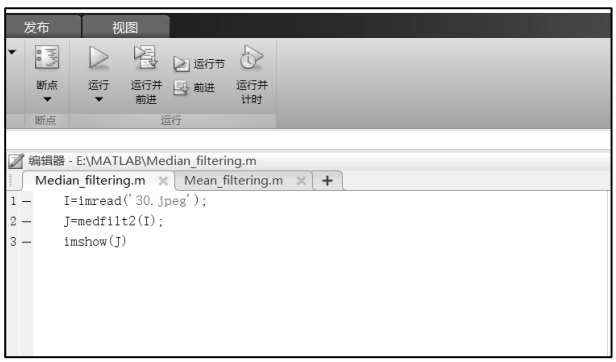

Fig. 8 *Median filtering program diagram (*$J = medfilt2(I)$*)*

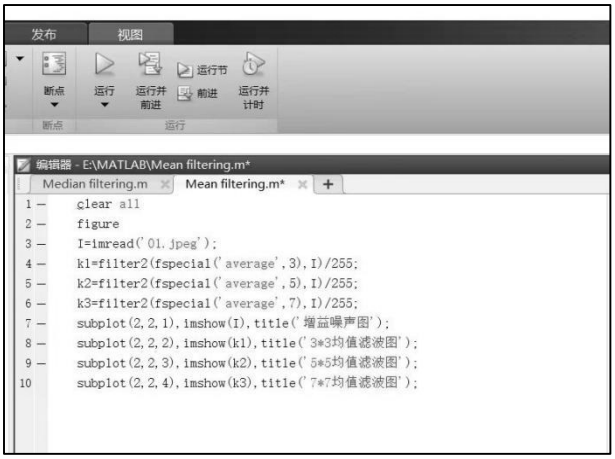

Fig. 9 *Average filtering program diagram (*$k = filter2(B, I)$*)*

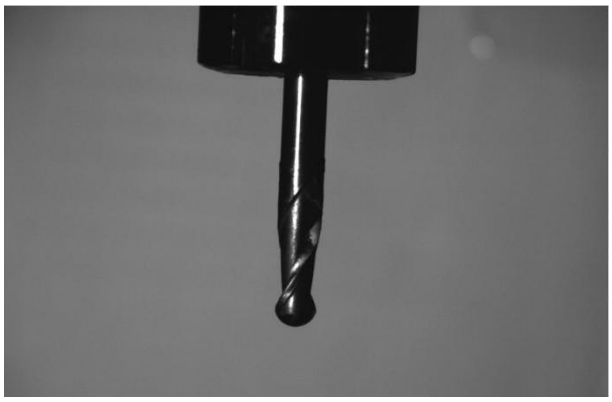

Fig. 10 *Pre-processed image after median filtering process*

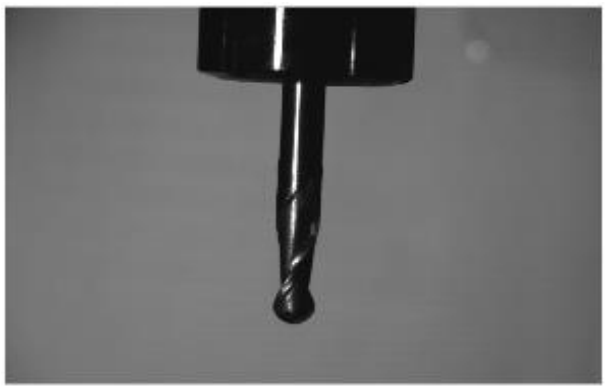

Fig. 11 *Pre-processed image after equalization process*

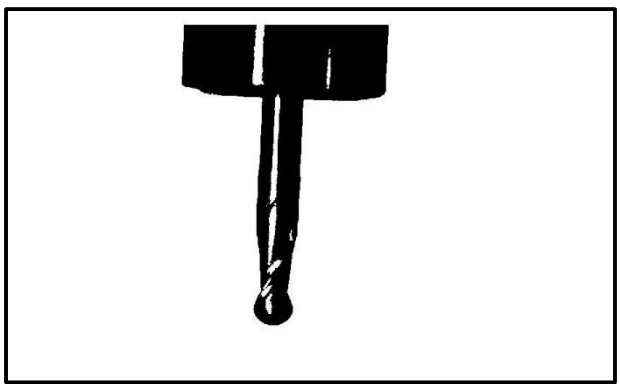

Fig. 12 *Pre-processed image after binarization process*

Binary processing of the image, which can make a significant difference between black and white. Normally, in two dimensions, each pixel in an image has a position that corresponds to it and also has a sample value associated with it, which may be one or more. It is selected with a range constrained to 256 levels, that is, a gray scale threshold [0 (black) to 255 (white)]. In this way, a binary image is obtained that reflects the properties of the image[24].

According to the gray level of the image, by the method of Maximization of inter-class variance， it is divided into two parts, one of which is the background and the other the target. When the variance value between the two is greater, the less likely it is that the target will be incorrectly assigned. The tool images captured in this paper have a large gray scale step between the tool and the background，and the inter-class variance values are large，so the maximum inter-class variance method is more suitable for partitioning. And this method can process the images efficiently and quickly, with a small calculating volume, suitable for batch processing of multiple images, which meets the demand for image processing techniques later in this paper. Therefore, this method is chosen for binary processing of the images captured afterwards.

During the experiment, the high-speed camera took pictures for 2-min periods, the machine spindle speed was 1000 r/min and the machine ran for 0.5 h. The images were pre-processed with median filtering, histogram equalization and binary processing, and the results are shown in Fig. 10-12.

4.2 Edge extraction of tool images

For the pre-processed images, we need to detect the edge contours and determine the location of all edge pixels. In the process of tool edge processing, common edge detection operators are Roberts operator, Sobel operator, Prewitt operator, Log operator, Canny operator, etc. The detection of edges by each operator is shown in Tab. 2[25-26].

Tab. 2 *Detection of edges by each operator*

Algorithm	Application
Roberts	Good at processing images with steep, low noise, but edge location is not very accurate. More suitable for horizontal and vertical edge detection.
Sobel	It has a smoothing effect on the noise and can provide more accurate information on the direction of the edges, but the accuracy of edge positioning is not high. When accuracy is not required, this operator can be used for image edge detection.
Prewitt	It has a smoothing effect on noise but low positioning accuracy. It is better for images with gradual gray scale and more noise.
Log	The Laplace Gaussian algorithm often has double pixel boundaries and the detection method is sensitive to noise, so it is rarely used to detect edges, instead it is used to determine whether the edge pixels are located in the bright or dark areas of the image.
Canny	This algorithm is not easily disturbed by noise. It has good de-noising ability and produces finer edges. But it also tends to smooth out some edge information.

Analyzing the above algorithms together, the Canny algorithm detects edges by finding local maximums of the image gradient, calculating the gradient with first order differentiation of the Gaussian function, and using 2 thresholds to detect strong and weak edges respectively. When and only when the weak edge is connected to the strong edge, the weak edge is output, and is not easily disturbed by noise, which can achieve a better balance between noise and edge detection. Thereby detecting the real weak edge. It is more suitable for the follow-up processing of the experiment in the paper, so the Canny operator is used.

4.2.1 Canny algorithm detection principle

The algorithm is a multistage optimization operator with filtering, enhancing and detecting. The Canny operator first uses a Gaussian smoothing filter to smooth the image to remove noise, uses a first-order partial derivatives with finite differences to calculate the gradient amplitude and direction, goes through a non-maximum suppression process during processing, and finally uses two thresholds to connect the edges.

In this paper, the Canny operator in the MATLAB edge detection function Edge is called so as to achieve the initial positioning of the tool edge profile. The MATLAB program statement is shown in Equation 3.

$$pic = edge(pic, 'Canny', 0.15) \quad (3)$$

Where:

Pic…The matrix that stores the image data,

Canny…The arithmetic in the edge function,

0.15…The high threshold value that is used to link the image edges into contours, and when the endpoint of the contour is reached, the algorithm looks for a point that satisfies the low threshold among the 8 neighbour points of the break point, and then collects new edges based on this point until the entire image edge is closed.

4.2.2 Sub-pixel fitting algorithm

Although the Canny arithmetic can detect true weak edges, but it can only do whole pixel edge detection. Therefore, in order to further improve the accuracy of image outline detection. Therefore, in order to

further improve the accuracy of image contour detection, coarse localization of the Canny operator followed by sub-pixel fine localization，which not only can effectively avoid noise interference, but also can improve the accuracy of edge detection.

The sub-pixel is a further subdivision of the basic unit of the pixel, using computer software and corresponding algorithms to calculate the accuracy that cannot be achieved by hardware, thus improving the image resolution in software terms[27].In general, sub-pixel edge points exist in areas of the image where transitions change gradually, and the sub-pixel positions of edge points can be obtained using a variety of methods such as polynomial fitting. Sub-pixel positioning can be understood as a method of using software algorithms to improve edge detection accuracy while the hardware conditions of the camera system remain unchanged, or as an image processing technique that allows for a resolution of less than one pixel.

Edge detection algorithms at the sub-pixel level can be grouped into 3 types: moment methods, interpolation methods and fitting methods. The fitting method does not require numerical differentiation and is fitted by minimizing the distance from each gray value to the fitted curve. This not only makes reasonable use of the gray values with errors, but also reduces the effect of gray value errors, so the fitting method is insensitive to noise. Therefore, this paper uses the proposed method for sub-pixel localization of images.

The Polyfit function in MATLAB is called to perform a sub-pixel fit to the image (as shown in Equation 4). and the fit function is shown in Fig. 13 with the following program statement.

$$p = polyfit(x, y, n) \tag{4}$$

Where:

p…The coefficient that returns,

n…Order polynomial p(x) that is the best fit to the data in y(in least squares).

p(x) is calculated as shown in Equation 5.

$$p(x) = p_1 x^n + p_2 x^{n-1} + \cdots + p_n x + p_{n+1} \tag{5}$$

After pre-processing the image, the edge outline of the milling cutter is extracted using the Canny algorithm as shown in Fig. 14. The tool outline curve was fitted using the sub-pixel fitting method as shown in Fig. 15.

```
clear x;
clear y;
x=[ ]; y=[]; i=1;
figure(1)， imshow(~result);
[mouse_y， mouse_x]=gin put(2);
for ii=1 : k
    if x1(ii)>min(mousc_x)&&x1(ii)⩽max(mousc)
        x(i)=x1(ii);
        y(i)=y1(ii);
        i=i+1;
        end
end
j=1;
kkk=polyfit(y,x,2); % Fitting the curve with polyfit
aaa(j,1)=kkk(1， 1);
aaa(j,2)=kkk(1， 2);
aaa(j,3)=kkk(1,3);
```

Fig. 13 *Polyfit fitting function*

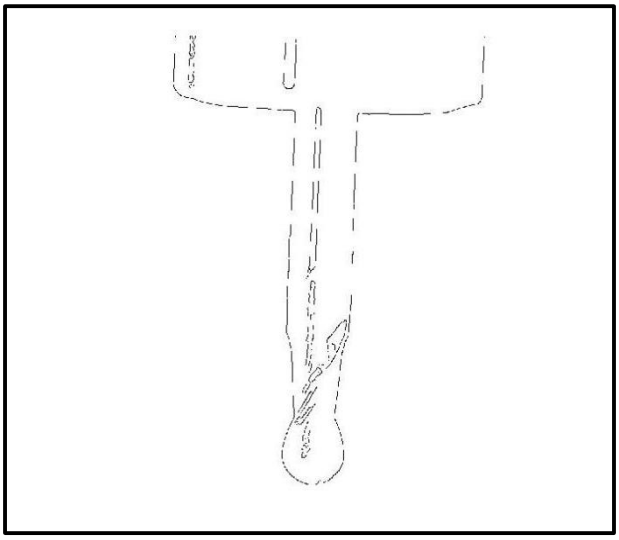

Fig. 14 *Milling cutter edge outline*

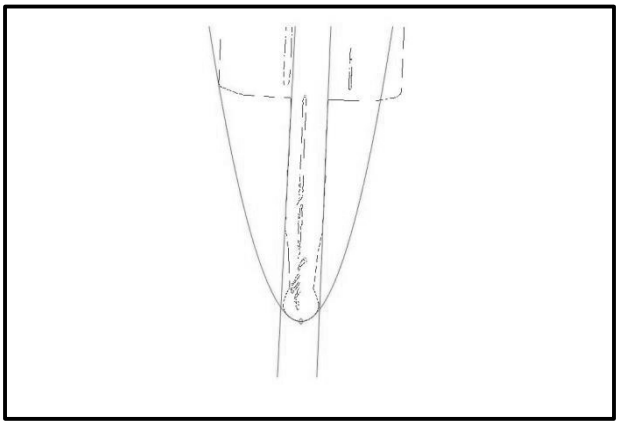

Fig. 15 *Sub-pixel fitted outline*

4.3 Edge extraction of tool images

Using the point to line distance Equation 6, applying the point to line distance equation (2), the distance between the lowest point of the fitted tool tip and the reference line is calculated, thereby obtaining the amount of axial tool heat deflection.

$$d = \frac{\left| \ Ax_0 + By_0 + C \ \right|}{\sqrt{A^2 + B^2}} \tag{6}$$

Following the steps as above, the experimental data was obtained as shown in Tab. 3.

Tab. 3 *Experimental Data Sheet*

No.	Time/*min*	Tool y-axis difference/*pixel*
0	0	542.5244
1	2	543.0588
2	4	543.0648
3	6	543.3291
4	8	543.3147
5	10	543.3638
6	12	543.6729
7	14	543.4659
8	16	543.4999
9	18	543.6384
10	20	543.6478
11	22	543.6654
12	24	543.6709
13	26	543.6816
14	28	543.7165
15	30	543.7222

Fitting the scatter of the variation data of the tool thermal deformation values, the results are shown in Fig. 16.

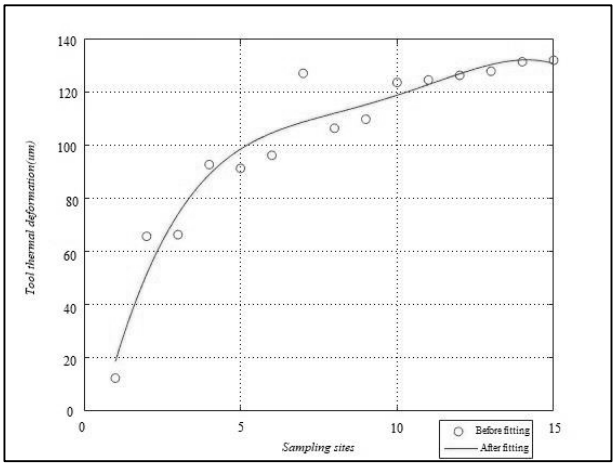

Fig. 16 *Tool thermal deformation fitting curve*

From the fitting results, it can be seen that: in the first 0~6 min, the tool axial thermal deformation is large; in the 6th~26 min, the tool thermal deformation gradually becomes smaller; in the preheating time of the 26th min, the tool deformation reaches more than 96% of the total deformation, while the fitting curve gradually tends to level off and the tool deformation gradually gets stable, at this time the tool thermal deformation is 130.2 um.

5 Conclusions

Aiming at the problem of thermal deformation of tools during the preheating process of machine tools, a method of measuring thermal deformation of tools based on image processing technology is proposed. The tool images of the preheating stage of the high-speed machining center are captured in time. The images captured by the high-speed camera are pre-processed with filtering, image histogram enhancement and binarization. Using the position coordinates at the tool tip as the main measurement parameter, the Canny algorithm and sub-pixel fitting method are used to achieve effective measurement of the deformation of high-speed rotating tools during the preheating process. The experimental results showed that: the tool in the machine preheating process, its thermal deformation increased with the machine running time, and in the preheating of the 26 min tool deformation reached more than 96% of the total deformation, and the deformation rate tends to be stable. The axial deformation of the tool at this point was measured to be 130.2 um. The results of this study can be applied to the actual production machining of CNC machine tools. This can shorten the warm-up time of processing and tool change period, reduce the machining errors caused by thermal errors in the actual production of CNC machine tools. So as to improve the efficiency and accuracy of CNC machine tools, and reduce processing costs.

References

[1] YU, H., JIANG, L., WANG, J., QIN, S., & DING, G. (2020). Prediction of machining accuracy based on geometric error estimation of tool rotation profile in five-axis multi-layer flank milling process. In: Proceedings of the Institution of Mechanical Engineers, Part C: *Journal of Mechanical Engineering Science*, 234(11), 2160-2177. England. ISSN:2041-2983

[2] ZHAO, G., SU, Y., ZHENG, G., ZHAO, Y., & LI, C. (2020). Tool tip cutting specific energy prediction model and the influence of machining parameters and tool wear in milling. Proceedings of the Institution of Mechanical Engineers, Part B: *Journal of Engineering Manufacture*, 234(10), 1346-1354. England. ISSN:2041-2975

[3] YANG, M., DAI, Y., HUANG, Q., MAO, X., LI, L., JIANG, X., & PENG, Y. (2019). A modal parameter identification method of machine tools based on particle swarm

optimization. Proceedings of the Institution of Mechanical Engineers, Part C: *Journal of Mechanical Engineering Science*, 233(17), 6112-6123. England. ISSN:2041-2983

[4] MAZNAH ILIYAS AHMAD, YUSRI YUSOF & MD ELIAS DAUD. (2020). Machine monitoring system: a decade in review. *The International Journal of Advanced Manufacturing Technology*, 108(11), 3645-3659. England. ISSN:0268-3768

[5] BAUM, C., BRECHER, C., KLATTE, M., LEE, T. H., & TZANETOS, F. (2018). Thermally induced volumetric error compensation by means of integral deformation sensors. *Procedia CIRP*, 72, 1148-1153. France. ISSN:2212-8271

[6] VASILKO, K. (2019) Tribological Mechanism in Chip Formation and Its Use to Improve Machining Process. *Manufacturing Technology*. 19(6), 1060-1066. Czech Republic. ISSN:1213-2489

[7] STANCEKOVA, D., RUDAWSKA, A., MRÁZIK, J., & TURIAN, F. (2020) Comparision of the Bearing Rings Deformation after Heat Treatment. *Manufacturing Technology*. 20(5), 677-683. Czech Republic. ISSN:1213-2489

[8] WIESSNER, M., BLASER, P., BÖHL, S., MAYR, J., KNAPP, W., & WEGENER, K. (2018). Thermal test piece for 5-axis machine tools. *Precision Engineering*, 52, 407 − 417. United States. ISSN:0141-6359

[9] MAREŠ, M., HOREJŠ, O., & HORNYCH, J. (2020). Thermal Error Minimization of a Turning-Milling Center with Respect to its Multi-Functionality. *International Journal of Automation Technology*, 14(3), 475-483. Japan. ISSN:1881-7629

[10] LIU, K., LI, T., LIU, H., LIU, Y., & WANG, Y. (2019). Analysis and prediction for spindle thermal bending deformations of a vertical milling machine. *IEEE Transactions on Industrial Informatics*, 16(3), 1549-1558. United States. ISSN:1551-3203

[11] PUTZ, M., REGEL, J., WENZEL, A., & BRÄUNIG, M. (2019). Thermal errors in milling: comparison of displacements of the machine tool, tool and workpiece. *Procedia CIRP*, 82, 389-394. France. ISSN:2212-8271

[12] MARCELO O. DOS SANTOS, GILMAR F. BATALHA, ED C. BORDINASSI, & GELSON F. MIORI. (2018). Numerical and experimental modeling of thermal errors in a five-axis CNC machining center. *The International Journal of Advanced Manufacturing Technology*, 96(5), 2619-2642. Germany, ISSN:1433-3015

[13] YE, W. H., GUO, Y. X., ZHOU, H. F., LIANG, R. J., & CHEN, W. F. (2020). Thermal error regression modeling of the real-time deformation coefficient of the moving shaft of a gantry milling machine. *Advances in Manufacturing*, 8(1), 119-132. China. ISSN:2095-3127

[14] LAMBIASE, F., PAOLETTI, A., & DI ILIO, A. (2018). Forces and temperature variation during friction stir welding of aluminum alloy AA6082-T6. *The International Journal of Advanced Manufacturing Technology*, 99(1), 337-346. England. ISSN:0268-3768

[15] YUE, H. T., GUO, C. G., LI, Q., ZHAO, L. J., & HAO, G. B. (2020). Thermal error modeling of CNC milling machining spindle based on an adaptive chaos particle swarm optimization algorithm. *Journal of the Brazilian Society of Mechanical Sciences and Engineering*, 42(8), 1-13. Brazil. ISSN:1678-5878

[16] YONGLUN CHEN HUAIAN YI CHEN LIAO PENG HUANG QIUCHANG CHEN. (2021). Visual measurement of milling surface roughness based on Xception model with convolutional neural network. *Measurement*, 186, 110217. England. ISSN:0263-2241

[17] MALHOTRA, J., & JHA, S. (2021). Fuzzy c-means clustering based colour image segmentation for tool wear monitoring in micro-milling. *Precision Engineering*, 72, 690-705. United States. ISSN:0141-6359

[18] PENG, R., LIU, J., FU, X., LIU, C., & ZHAO, L. (2021). Application of machine vision method in tool wear monitoring. *The International Journal of Advanced Manufacturing Technology*, 116(3), 1357-1372. England. ISSN:0268-3768

[19] BRADY, D. J., FANG, L., & MA, Z. (2020). Deep learning for camera data acquisition, control, and image estimation. *Advances in Optics and Photonics*, 12(4), 787-846. United States. ISSN:1943-8206

[20] XIAO, M., SUN, Z., SHEN, X., SHI, L., & ZHANG, J. (2019). Research on 3d reconstruction technology of tool wear area. *Manufacturing Technology*, 19(2), 345-349. Czech Republic. ISSN:1213-2489

[21] ANJAR WANTO, SYAFRIKA DENI RIZKI & SILFIA ANDINI. (2020). Combination of Sobel+Prewitt Edge Detection Method with Roberts+Canny on Passion Flower Image Identification. *Journal of Physics: Conference Series*,1933(1), 012037. England. ISSN:1742-6596

[22] DUTTA, S., PAL, S. K., & SEN, R. (2018). Progressive tool condition monitoring of end milling from machined surface images. Proceedings of the Institution of Mechanical Engineers, Part B: *Journal of Engineering Manufacture*, 232(2), 251-266. England. ISSN:0954-4054

[23] CHARMOUTI, B., JUNOH, A. K., ABDURRAZZAQ, A., & MASHOR, M. Y. (2022). A new denoising method for removing salt & pepper noise from image. *Multimedia Tools and Applications*, 81(3), 3981-3993. Netherlands. ISSN:1380-7501

[24] RUITAO PENG, HAOLIN PANG & HAOJIAN JIANG. (2020). Study of tool wear monitoring using machine vision. *Automatic Control and Computer Sciences*, 54(3), 259-270. United States. ISSN:0146-4116

[25] LIU, Y., ZHANG, Q., CHEN, Y., CHENG, Q., & PENG, C. (2021). Hyperspectral Image Denoising With Log-Based Robust PCA. *2021 IEEE International Conference on Image Processing Proceedings*, 1634-1638. United States. ISSN:2381-8549

[26] MÜLLER, J., WITTIG, R., MÜLLER, J., & TETZLAFF, R. (2016). An improved cellular nonlinear network architecture for binary and grayscale image processing. *IEEE Transactions on Circuits and Systems II: Express Briefs*, 65(8), 1084-1088. United States. ISSN:1549-7747

[27] KUMAWAT, A., & PANDA, S. (2021). A robust edge detection algorithm based on feature-based image registration (FBIR) using improved canny with fuzzy logic (ICWFL). *The Visual Computer*, 1-22. Germany. ISSN:1432-2315